Journal of Sound and Vibration 332 (2013) 3315–3328

Contents lists available at SciVerse ScienceDirect

Journal of Sound and Vibration

journal homepage: www.elsevier.com/locate/jsvi

Development of physical-parameter identification procedure for in-situ buildings with sliding-type isolation system

Ming-Chih Huang [a,*], Yen-Po Wang [b], Tzu-Kang Lin [b], Yi-Hsuan Chen [b]

[a] Department of Aircraft Engineering, Air Force Institute of Technology, 1, Jyulun Road, Gangshan District, Kaoshiung City 820, Taiwan, ROC

[b] Department of Civil Engineering, National Chiao Tung University, Hsinchu, 300, Taiwan, ROC

ARTICLE INFO

Article history:
Received 7 June 2012
Received in revised form
6 December 2012
Accepted 10 January 2013
Handling Editor: K. Shin
Available online 5 February 2013

ABSTRACT

A system identification procedure is developed to identify the physical parameters of structures with seismic isolation using the friction pendulum systems (FPSs). The superstructure is assumed to be linear on account of substantial reduction of seismic forces with the installation of FPS. Hysteretic models of both Coulomb's and Mokha's friction mechanism have been considered for the FPS. Simulation results indicate that the physical parameters of the FPS and superstructure can be successfully identified by the proposed scheme. Experimental verification has been conducted further via shaking table tests using realistic earthquake scenarios. The identified parameters from seismic response data indicate that the FPSs behave in better agreement with Mokha's friction mechanism than Coulomb's. Feasibility of the proposed scheme in the identification of FPS-isolated structures using seismic data has been verified. This may facilitate in-situ performance assessment of structures isolated with sliding-type isolation systems.

1. Introduction

A variety of seismic isolation devices have been developed and adopted for seismic protection of buildings, bridges and storage tanks in the past two decades [1–9]. Moreover, the seismic isolation device in conjunction with the MR dampers have also been studied for response mitigation of adjacent buildings [10].

Design guidelines and building codes have been established to facilitate the design and standardize the construction of structures employing base isolation systems. Among the seismic isolation systems that have been adopted in practice, the Friction Pendulum System (FPS) has drawn a great deal of attention [11–15]. The FPS utilizes a concaved sliding surface to generate a restoring force as displaced while changing the fundamental period of the isolated structure in the sliding mode. Previous research on FPS has been focusing on developing simplified models or constitutive relations to validate the performance and behavior of the isolation systems [16–22]. In the meantime, applications of FPS on diverse structures were also prosperously studied. For example, Ates et al. [23] studied the effect of spatially varying earthquake ground motions on the stochastic response of bridges isolated with FPS. Kunde and Jangid [24] studied the influence of pier and deck flexibility on seismic response of bridges isolated by both the elastomeric bearings and FPS, and the inelastic force–displacement relation of the FPS of seismically isolated bridges was approached by a time-dependent equivalent linearization technique [25]. Marin-Artieda et al. [26] studied the response of structures isolated with XY-friction

* Corresponding author. Tel.: +886 7 6254168; fax: +886 6 3357 663.
E-mail address: sander.huang@msa.hinet.net (M.-C. Huang).

0022-460X/$ - see front matter © 2013 Elsevier Ltd. All rights reserved.
http://dx.doi.org/10.1016/j.jsv.2013.01.013

Nomenclature

a	bearing pressure
a^l	l-th iteration of the bearing pressure
C_j	damping coefficient of the j-th floor
C_1^n	n-th iteration of the damping coefficient of the first floor
e_1	first measure-of-fit of the base
e_2	second measure-of-fit of the base
e	overall measure-of-fit of the base
e_{Fj}	measure-of-fit of the j-th floor
$f_r(\bullet)$	restoring force of the friction pendulum systems (FPSs)
K_j	stiffness of the j-th floor
K_1^m	m-th iteration of the stiffness coefficient of the first floor
m_0	mass of the base
m_j	mass of the j-th floor
R	curvature radius of the FPS
W	total weight of the structure
x_0	displacement of the base
$\dot{x}_0$	velocity of the base
$\dot{x}_0$	acceleration of the base
x_0^i	displacement of the base at instant i
$\dot{x}_0^i$	velocity of the base at instant i
$\ddot{x}_0^i$	acceleration of the base at instant i
x_j	displacement of the j-th floor
$\dot{x}_j$	velocity of the j-th floor
$\ddot{x}_j$	acceleration of the j-th floor
x_j^i	displacement of the j-th floor at instant i
$\dot{x}_j^i$	velocity of the j-th floor at instant i
$\ddot{x}_j^i$	acceleration of the j-th floor at instant i
$\ddot{x}_g$	ground acceleration
Δa	increment of the bearing pressure coefficient
$\Delta C_1^{(s)}$	increment of the damping coefficient of the first floor set for the sth cycle
$\Delta K_1^{(s)}$	increment of the stiffness coefficient of the first floor set for the sth cycle
μ	friction coefficient of the FPS
μ_{max}	maximum friction coefficient of the FPS
μ_{min}	minimum friction coefficient of the FPS

pendulum (XY-FP) systems under tri-axial excitations. The XY-FP bearings were demonstrated to be resistant of tensile loads. Kim et al. [27] studied the feasibility of using FPS bearings for seismic isolation of spatial lattice shell structures.

As more and more seismic isolation systems have been implemented for practical use, the in-situ identification of the bearing parameters and monitoring of the isolation performance has become a critical issue. The seismic structural response data recorded during earthquake episodes indeed provide valuable information on the dynamic characteristics of the structures if accurately identified. As most of the isolation systems are nonlinear in nature, time-domain and physical-parameter identification approach is preferred. For example, Nagarajaiah and Xiaohong studied the responses of a base-isolated hospital building in the University of Southern California (USC) and the Fire Command and Control (FCC) building by using a bilinear model for the base isolation system and a three-dimensional analytical models that accounted for the effects of eccentric impact loading with respect to the center of mass to estimate the lateral-torsional response of the base-isolated building, respectively [28,29]. The simulation results based on the identified parameters and the proposed analytical model were in good agreement with the recorded data, and the seismic performance of the buildings was proved satisfactory. A base-isolated structure with bi-axial seismic response data was identified by Furukawa et al. [30] using a prediction error method (PEM) with a nonlinear state-space model of several inelastic restoring force–displacement models representing the base isolation system. Results indicated that the tri-linear hysteretic multiple shear spring (MSS) model best fitted the actual hysteretic restoring force profile and the recorded time histories. Recently, a procedure in time domain and frequency domain for the identification of structural systems with combined viscous and friction damping devices was proposed and applied on a base-isolated building using acceleration data recorded during free-vibration tests. In spite of the complexity of the isolation systems with coupled sliding and rubber bearings, the identified parameters compared favorably with those obtained by other methods [31]. A time-domain procedure for the identification of base isolation systems of both the high damping rubber bearing (HDRB) and low-friction sliding bearing (LFSB), where a constant Coulomb friction device was considered for the LFSB system was further developed [32]. The proposed procedure was applied to a hybrid isolation system, and the identified results from static and dynamic tests were in good agreement with those obtained from laboratory tests.

Up to date, most researches regarding the system identification of based-isolated structures are directed towards those using elastomeric type bearings such as lead-rubber bearing (LRB) or HDRB. The existing methodologies, which are commonly composed of simplified linear models, however, cannot be applied directly for identification of structures isolated with FPSs, as the system becomes highly nonlinear due to the essence of friction mechanism. In this study, a system identification procedure is therefore developed to identify the physical parameters of base-isolated buildings equipped with FPSs. Hysteretic models of both Coulomb's and Mokha's friction mechanism have been considered for the FPS. Simulation results indicate that the physical parameters of the FPS and superstructure can be successfully identified by the proposed scheme. Experimental verification has been conducted further via shaking table tests using realistic earthquake scenarios. The identified parameters from seismic response data indicate that the FPSs behave in better agreement with Mokha's friction mechanism than Coulomb's. Feasibility of the proposed scheme in the identification of FPS-isolated structures using seismic data has been verified. This may facilitate in-situ performance assessment of

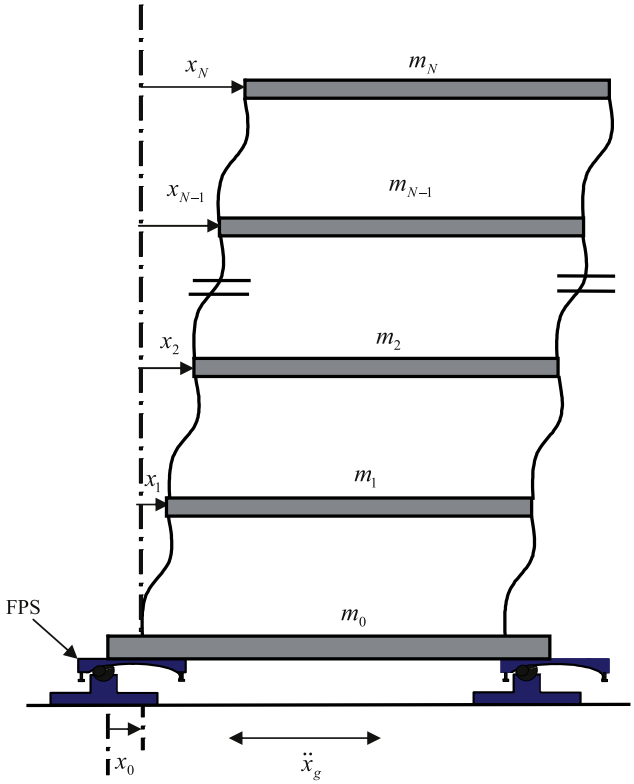

Fig. 1. FPS-Isolated building.

structures isolated with sliding-type isolation systems. This nonlinear parameter identification technique, in addition, may provide a possible means for the physical parameter identification of vehicle suspension systems of a nonlinear nature [33,34].

2. Motion equation

Consider a linear N-storey shear type structure mounted on a base-isolated foundation with FPSs, as shown in Fig. 1. Due to the hysteretic and energy-absorbing effects of FPSs, the dynamic behavior of the superstructure is presumed to be linear. The equation of motion of the superstructure can be expressed as

$$m_N\ddot{x}_N+C_N(\dot{x}_N-\dot{x}_{N-1})+K_N(x_N-x_{N-1})=-m_N(\ddot{x}_g+\ddot{x}_0) \tag{1}$$

$$\begin{aligned} &m_{j-1}\ddot{x}_{j-1}+C_{j-1}(\dot{x}_{j-1}-\dot{x}_{j-2})+K_{j-1}(x_{j-1}-x_{j-2})\\ &-C_j(\dot{x}_j-\dot{x}_{j-1})-K_j(x_j-x_{j-1})=-m_{j-1}(\ddot{x}_g+\ddot{x}_0)\quad j=3\sim N \end{aligned} \tag{2}$$

$$m_1\ddot{x}_1+C_1\dot{x}_1+K_1x_1-C_2(\dot{x}_2-\dot{x}_1)-K_2(x_2-x_1)=-m_1(\ddot{x}_g+\ddot{x}_0) \tag{3}$$

and for the base

$$m_0\ddot{x}_0-C_1\dot{x}_1-K_1x_1=-m_0\ddot{x}_g+f_r(x_0,\dot{x}_0) \tag{4}$$

where x_j is the displacement of the j-th floor of the structure in relation to the base; x_0 is the displacement of the base in relation to the ground; m_j and m_0 are the mass of the j-th floor and the base, respectively; C_j and K_j are the damping coefficient and stiffness of the j-th floor; $\ddot{x}_g$ is the ground acceleration; $f_r(x_0,\dot{x}_0)$ is the restoring force provided by the FPSs.

3. Friction mechanisms

The restoring force, $f_r(x_0,\dot{x}_0)$, in the sliding state of the FPS can be represented as

$$f_r(x_0,\dot{x}_0)=-\mathrm{sgn}\,(\dot{x}_0)\mu W-\frac{W}{R}x_0 \tag{5}$$

where x_0 is the displacement of the base relative to the ground; W is the total weight of the structure; μ and R are respectively the friction coefficient and curvature radius of the FPS.

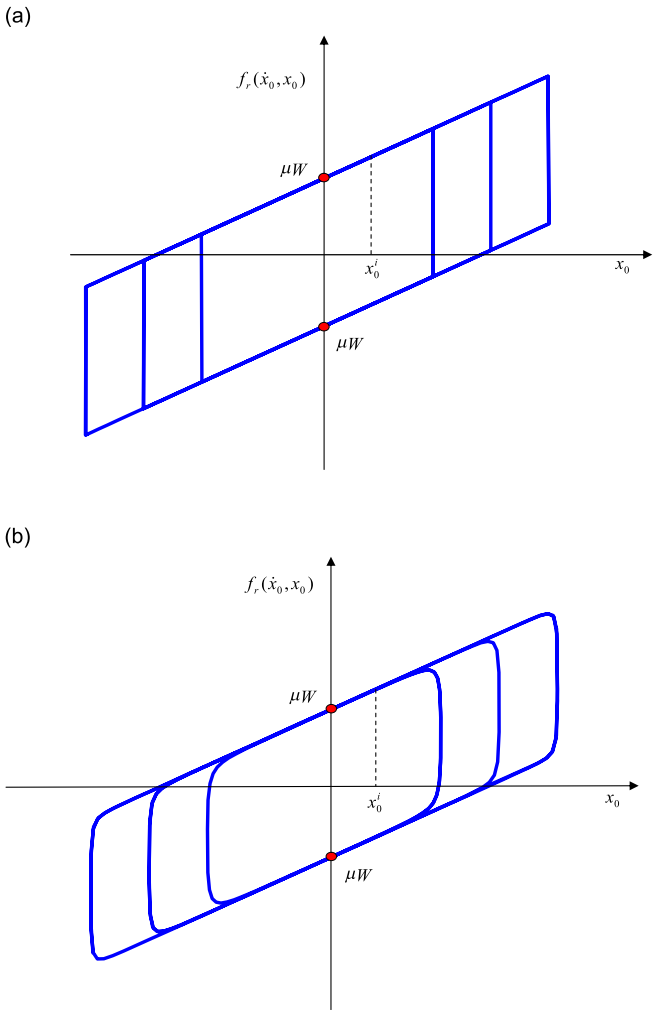

Fig. 2. (a) Hysteretic loop of FPS (Coulomb's mechanism) and (b) hysteretic loop of FPS (Mokha's mechanism).

The friction mechanism is commonly assumed to be of Coulomb's type with a constant friction coefficient, referred to as Coulomb's mechanism herein. Mokha et al. [35,36] proposed that the friction coefficient was dependent on the sliding velocity of the bearings ($\dot{x}_0$) as well as the bearing pressure. It was expressed in an empirical form of

$$\mu = \mu_{\max} - (\mu_{\max} - \mu_{\min}) e^{-a|\dot{x}_0|} \tag{6}$$

where μ_{max} and μ_{min} are the maximum and minimum friction coefficients; a is bearing pressure related coefficient; $\dot{x}_0$ is the relative velocity between the slipping interfaces. This is referred to as "Mokha's mechanism" in this paper. The hysteretic models of the two different mechanisms are shown in Fig. 2(a) and (b).

Substituting Eq. (5) for $f_r(x_0,\dot{x}_0)$ into Eq. (4), the equilibrium equation of the base at instant i becomes

$$\ddot{x}_0^i + \operatorname{sgn}\left(\dot{x}_0^i\right)\frac{\mu W}{m_0} + \frac{W}{Rm_0}x_0^i = \ddot{u}_g^i \tag{7}$$

where

$$\ddot{u}_g^i = -\ddot{x}_g^i + \frac{C_1}{m_0}\dot{x}_1^i + \frac{K_1}{m_0}x_1^i \tag{8}$$

4. Solution algorithms for physical parameter identification

The output-error technique that determines the system parameters by minimizing the discrepancies between the output and predictive values will be adopted [37,38]. When the responses of all the floors (including the base) are measured, the physical parameters of the FPS-isolated structure can be identified provided that the masses for all the floors are known.

4.1. Output-error functions for the FPS

Eq. (7) is the key equation for identifying the physical parameters of the FPS system. Prior to the identification process, all the available dynamic response data are classified into two groups in accordance with the direction of the sliding velocity, that is sgn $(\dot{x}_0)$. To avoid complication in dealing with highly nonlinearity around the reversals of motion direction, for those $|\dot{x}_0^i| < 0.01\ m/s$ are abandoned in the analysis.

4.1.1. Coulomb's mechanism

For the set of data with $\dot{x}_0^i \geq 0.01\ m/s$, the first measure-of-fit, e_1, is defined by the sum of square errors using Eq. (7) with $\ddot{u}_g^i$ determined from Eq. (8) for a specified set of C_1 and K_1 as

$$e_1 = \sum_i \left[\ddot{x}_0^i + \frac{\mu W}{m_0} + \frac{W}{Rm_0}x_0^i - \ddot{u}_g^i\right]^2 \tag{9}$$

Similarly, for the data set with $\dot{x}_0^j \leq -0.01\ m/s$, the second measure-of-fit, e_2, is defined by the sum of square errors as

$$e_2 = \sum_j \left[\ddot{x}_0^j - \frac{\mu W}{m_0} + \frac{W}{Rm_0}x_0^j - \ddot{u}_g^j\right]^2 \tag{10}$$

Provided that the total weight of the structure, W, and the mass of the base, m_0, are known, μ and R are then obtained by simultaneously solving for the system equation from minimization of the overall measure-of-fit

$$e = e_1 + e_2 \tag{11}$$

as

$$\frac{\partial e}{\partial(\mu W/m_0)} = 0; \quad \frac{\partial e}{\partial(W/Rm_0)} = 0 \tag{12}$$

A two-layered nested structure is considered for the solution algorithm. The identification procedure starts by assuming an arbitrary initial value of C_1 with K_1 incrementally changed in Eq. (8). The local optimal K_1 corresponds to that giving the minimum of e. Then, K_1 is fixed at this local optimal value and the process is proceeded by incrementally changing C_1 in Eq. (8) to find the local optimal C_1. Meanwhile, the corresponding system parameters μ and R are alternately determined for each set of K_1 and C_1 from Eq. (12). This is termed as one complete "cycle" of sweeping analysis. The procedure may be continued using smaller resolutions of the parameters within a reduced scope until convergence has been achieved. The number of cycles needed in the analysis depends on the desired resolution of the parameters.

4.1.2. Mokha's mechanism

For the set of data with $\dot{x}_0^i \geq 0.01\ m/s$, the first measure-of-fit, e_1, is defined by the sum of square errors using Eq. (7) with a specified a and $\ddot{u}_g^i$ determined from Eq. (8) for a specified set of C_1 and K_1 as

$$e_1 = \sum_i \left[\ddot{x}_0^i + \left(\mu_{\max} - (\mu_{\max} - \mu_{\min})e^{-a|\dot{x}_0^i|}\right)\frac{W}{m_0} + \frac{W}{Rm_0}x_0^i - \ddot{u}_g^i\right]^2 \tag{13}$$

Similarly, for the data set with $\dot{x}_0^j \leq -0.01\ m/s$, the second measure-of-fit, e_2, is defined by the sum of square errors as

$$e_2 = \sum_j \left[\ddot{x}_0^j - \left(\mu_{\max} - (\mu_{\max} - \mu_{\min})e^{-a|\dot{x}_0^j|}\right)\frac{W}{m_0} + \frac{W}{Rm_0}x_0^j - \ddot{u}_g^j\right]^2 \tag{14}$$

μ_{max}, μ_{min} and R are then obtained by simultaneously solving for the system equation from minimization of the overall measure-of-fit e defined in Eq. (11) as

$$\frac{\partial e}{\partial(\mu_{\max} W/m_0)} = 0; \quad \frac{\partial e}{\partial(\mu_{\min} W/m_0)} = 0; \quad \frac{\partial e}{\partial(W/Rm_0)} = 0. \tag{15}$$

A three-layered nested structure is adopted for the solution algorithm. The identification procedure starts by assuming an arbitrary initial value of C_1 with K_1 incrementally changed in Eq. (8). The local optimal K_1 corresponds to that giving the minimum of e at a given a. Then, K_1 is fixed at this local optimal value and the process is proceeded by incrementally changing C_1 in Eq. (8) to find the local optimal C_1. Meanwhile, the corresponding system parameters μ_{max}, μ_{min} and R are alternately determined for each set of K_1 and C_1 from Eq. (15) at a given a value. In the outermost sweeping level, a is further incrementally changed for Eqs. (13) and (14) to find the local optimal a that minimizes e. Again, the procedure may be continued using smaller resolutions of the parameters within a reduced scope until convergence has been achieved.

4.2. Output-error functions for the superstructure

The parameters of the superstructure are consecutively identified level by level in a bottom-up fashion. For floor 2, the error function e_{F2} is defined by the sum of square errors using Eq. (3) with the optimal K_1 and C_1 obtained previously

determined as

$$e_{F2}=\sum_i\left[\ddot{x}_1^i+\frac{C_1}{m_1}\dot{x}_1^i+\frac{K_1}{m_1}x_1^i-\frac{C_2}{m_1}\left(\dot{x}_2^i-\dot{x}_1^i\right)-\frac{K_2}{m_1}\left(x_2^i-x_1^i\right)+\ddot{x}_g^i+\ddot{x}_0^i\right]^2 \tag{16}$$

Provided that the mass of Floor 1, m_1, is known, K_2 and C_2 are then obtained by simultaneously solving for the system equation from minimization of the measure-of-fit, e_{F2}, defined in Eq. (16) as

$$\frac{\partial e_{F2}}{\partial(C_2/m_1)}=0;\quad \frac{\partial e_{F2}}{\partial(K_2/m_1)}=0 \tag{17}$$

For floor $j\geq 3$, the error function e_{Fj} is defined by the sum of square errors using Eq. (2) with the optimal K_{j-1} and C_{j-1} obtained previously as

$$e_{Fj}=\sum_i\left[\ddot{x}_{j-1}^i+\frac{C_{j-1}}{m_{j-1}}\left(\dot{x}_{j-1}^i-\dot{x}_{j-2}^i\right)+\frac{K_{j-1}}{m_{j-1}}\left(x_{j-1}^i-x_{j-2}^i\right)-\frac{C_j}{m_{j-1}}\left(\dot{x}_j^i-\dot{x}_{j-1}^i\right)-\frac{K_j}{m_{j-1}}\left(x_j^i-x_{j-1}^i\right)+\ddot{x}_g^i+\ddot{x}_0^i\right]^2 \quad j=3\sim N \tag{18}$$

By the same token, K_j and C_j are then obtained by simultaneously solving for the system equation from minimization of the measure-of-fit, e_{Fj}, defined in Eq. (18) as

$$\frac{\partial e_{Fj}}{\partial(C_j/m_{j-1})}=0;\quad \frac{\partial e_{Fj}}{\partial(K_j/m_{j-1})}=0;\quad j=3\sim N \tag{19}$$

Thus all the physical parameters of the FPS and the structure are derived. The procedure of the identification process is summarized below:

Step 1: If Mokha's model is considered, the bearing pressure related coefficient a of the FPS is updated with $a^l=a^{l-1}+\Delta a$, where $\Delta a=9.81$. Skip this step if Coulomb's model is considered.
Step 2: Assume an initial value of C_1 with K_1 incrementally changed in Eq. (8) as $K_1^m=K_1^{m-1}+\Delta K_1^{(s)}$ for the m-th iteration, $\Delta K_1^{(s)}$ is the increment of the stiffness coefficient set for the s-th cycle.
Step 3(a): If Coulomb's mechanism is considered, solving for μ, R and K_1 by Eq. (12) based on the overall measure-of-fit e of Eq. (11). Go to Step 2 until run out a specified number of iterations. The local minima of μ, R and K_1 corresponds to the set giving the minimum e for all m.
(b): If Mokha's mechanism is considered, solving for μ_{min}, μ_{max}, R and K_1 by Eq. (15) based on the overall measure-of-fit e at a given a of Eq. (11). Go to Step 2 until run out of a specified number of iterations. Go to Step 1 until run out of a specified number of iterations for the outermost loop. The local minima of μ_{min}, μ_{max}, R and K_1 corresponds to the set giving the minimum e for all (m,l).
Step 4: With K_1 determined from Step 3, incrementally change C_1 in Eq. (8) as $C_1^n=C_1^{n-1}+\Delta C_1^{(s)}$ for the n-th iteration, $\Delta C_1^{(s)}$ is the increment of the damping coefficient set for the s-th cycle.
Step 5(a): If Coulomb's mechanism is considered, solving for μ, R and C_1 by Eq. (12) based on the overall measure-of-fit e of Eq. (11). Go to Step 4 until run out of a specified number of iterations. The local minima of μ, R and C_1 corresponds to the set giving the minimum e for all n.
(b): If Mokha's mechanism is considered, solving for μ_{min}, μ_{max}, R and C_1 by Eq. (15) based on the overall measure-of-fit e of Eq. (11) at a given a. Go to Step 4 until run out of a specified number of iterations. Go to Step 1 until run out of a specified number of iterations for the outermost loop. The local minima of μ_{min}, μ_{max}, R and C_1 corresponds to the set giving the minimum e for all (n,l).
Step 6: Repeat Steps 1–5 with updated initial values of C_1 and K_1 and the resolution $\Delta C_1^{(s)}=\Delta C_1^{(s-1)}/10$ and $\Delta K_1^{(s)}=\Delta K_1^{(s-1)}/10$ for $s=2,3,\ldots$ until the error converges. The optimal set of parameters K_1, C_1 , μ (or a, μ_{min} and μ_{max}) and R corresponds to the minimum e for all s.
Step 7: Determine C_j and K_j for $j=2\sim N$ of the superstructure by minimizing Eq. (16) or Eq. (18) based on the previously determined K_{j-1} and C_{j-1} of one storey below.

5. Numerical example

A 5-storey structure is considered for numerical simulation. The structure is modeled as a shear-type building with FPSs underneath its base as the isolation system. The physical parameters of the superstructure and base are as follows: $m_1=m_2=m_3=m_4=m_5=2000$ kg, and $m_0=1559$ kg; $C_1=7507.49$ kN.s/m, $C_2=7115.09$ kN.s/m, $C_3=7016.99$ kN.s/m, $C_4=6918.89$ kN.s/m, $C_5=6918.89$ kN.s/m; $K_1=29783.16$ MN/m, $K_2=27821.16$ MN/m, $K_3=23897.16$ MN/m, $K_4=22916.16$ MN/m, $K_5=19973.16$ MN/m. The parameters consider for the FPS are $R=2$ m and $\mu=0.1$ for Coulomb's mechanism and $\mu_{max}=0.1$, $\mu_{min}=0.5$ and $a=98.1$ for Mokha's mechanism. Dynamic responses of the base-isolated structure under the N–S component of

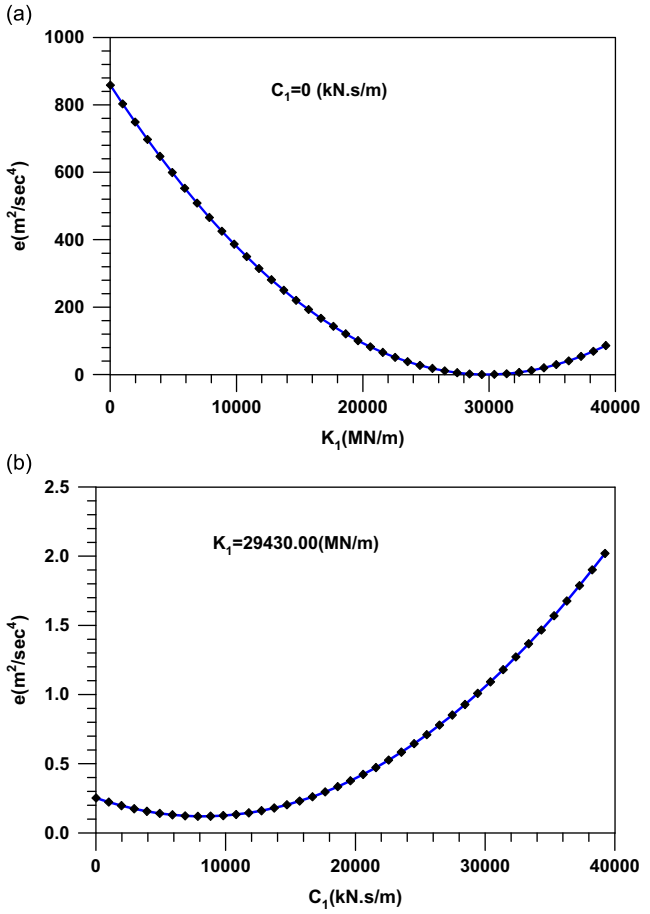

Fig. 3. (a) Measure-of-fit w.r.t. K_1 in the 1st cycle of iteration (numerical) and (b) measure-of-fit w.r.t. C_1 in the 1st cycle of iteration(Numerical).

the 1940 El Centro earthquake are determined using a state-space procedure with a time-step of 0.01 s. The velocity and displacement time histories were numerically integrated from the acceleration responses with a baseline correction.

5.1. Coulomb's mechanism

The first cycle ($s=1$) of the identification starts with $C_1=0$. The value of K_1 is increased by an increment of $\Delta K_1^{(1)}=981$ MN/m from 0 to 39240 MN/m. The relationship between the overall measure-of-fit e and K_1 is shown in Fig. 3(a). The optimal estimate of K_1 is found to be 29430.00 MN/m. Next, K_1 is fixed at this value and C_1 is increased by an increment of $\Delta C_1^{(1)}=981$ kN.s/m from 0 to 39240 kN.s/m. The relationship between the overall measure-of-fit e and C_1 is shown in Fig. 3(b). The optimal estimate of C_1 is found to be 7848.00 kN.s/m. Meanwhile, the parameters for FPSs are found to be $\mu=0.0989$ and $R=2.0053$ m.

The second cycle ($s=2$) of identification is then proceeded with $C_1=7848.00$ kN.s/m determined in the first cycle. The value of K_1 is increased by an increment of $\Delta K_1^{(2)}=\Delta K_1^{(1)}/10=98.1$ MN/m from 26487 to 32373 MN/m. The relationship between the overall measure-of-fit e and K_1 is shown in Fig. 4(a), and the optimal estimate of K_1 is found to be 29822.40 MN/m. Then, K_1 is fixed at29822.40 MN/m, and C_1 is increased by an increment of $\Delta C_1^{(2)}=\Delta C_1^{(1)}/10=98.1$ kN.s/m from 4905 to 8829 kN.s/m. The relationship between the overall measure-of-fit e and C_1 is shown in Fig. 4(b). The optimal estimate of C_1 is found to be 7455.60 kN.s/m. Meanwhile, the parameters for FPSs are found to be $\mu=0.1001$ and $R=1.9994$ m.

The identification results converge to the true values in five cycles as summarized in Table 1. The parameters for floor 2–5 of the superstructure are then calculated with an excellent accuracy as summarized in Table 2.

5.2. Mokha's mechanism

The iterative procedures in the inner cycles are similar to those for Coulomb's mechanism except for an additional loop of parameter a. To begin with, $\Delta a=9.81$ and $a^0=0$ are considered in $a^l=a^{l-1}+\Delta a$ where l is set to be 20 in this example. Again, the first cycle ($s=1$) starts with $C_1=0$. The value of K_1 is increased by an increment of $\Delta K_1^{(1)}=981$ MN/m. The least

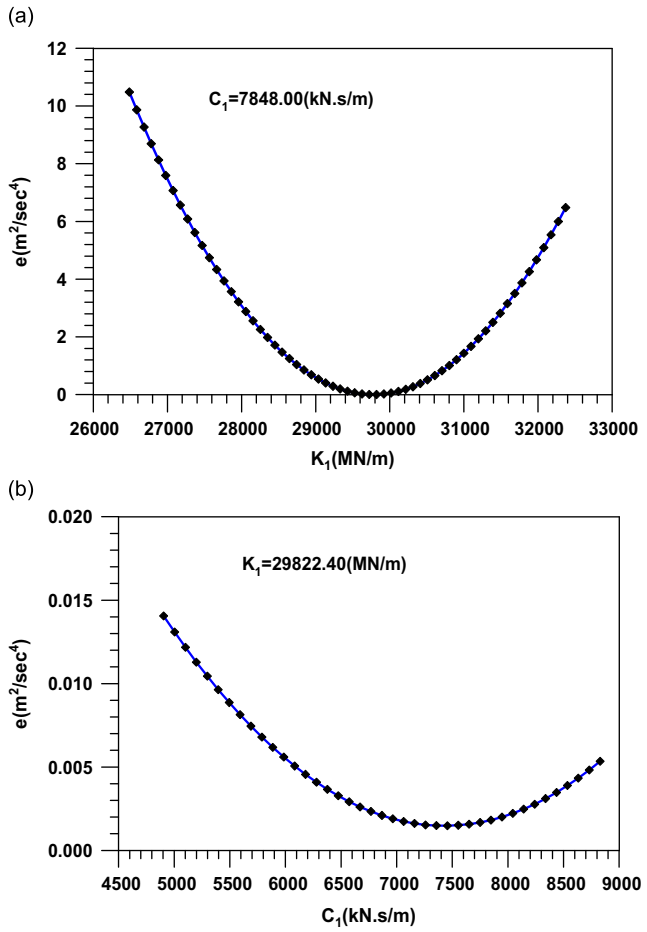

Fig. 4. (a) Measure-of-fit w.r.t. K_1 in the 2nd cycle of iteration (numerical) and (b) measure-of-fit w.r.t. C_1in the 2nd cycle of Iteration(Numerical).

Table 1
Parameters of FPS and floor 1 in numerical example (Coulomb's mechanism).

Iterative cycle (s)	μ	R (m)	C_1 (kN.s/m)	K_1 (MN/m)
1	0.0989	2.0053	7848.00	29430.00
2	0.1001	1.9994	7455.60	29822.40
3	0.1000	2.0000	7504.65	29783.16
4	0.1000	2.0000	7507.59	29783.16
5	0.1000	2.0000	7507.49	29783.16
True value	0.1000	2.0000	7507.49	29783.16

Table 2
Parameters of floor 2–5 in numerical example (Coulomb's mechanism).

Storey (j)	C_j (kN.s/m)		K_j (MN/m)	
	True	Identified	True	Identified
5	6918.89	6918.60	19973.16	19973.16
4	6918.89	6918.50	22916.16	22916.16
3	7016.99	7016.70	23897.16	23897.16
2	7115.09	7114.80	27821.16	27821.16

measure-of-fit occurs at $K_1=29430.00$ MN/m. Then, K_1 is fixed at this value with C_1 increased by an increment of $\Delta C_1^{(1)}=981$ kN.s/m in the iteration. The optimal estimate of C_1 is found to be 8829.00 kN.s/m at $a=98.1$. Meanwhile, the other parameters of the FPS are found to be $\mu_{max}=0.0989$, $\mu_{min}=0.0494$, and $R=2.0141$ m.

Table 3
Parameters of FPS and floor 1 in numerical example (Mokha's mechanism).

Iterative cycle (s)	a	μ_{max}	μ_{min}	R (m)	C_1 (kN.s/m)	K_1 (MN/m)
1	98.1	0.0989	0.0494	2.0141	8829.00	29430.00
2	98.1	0.0998	0.0499	2.0025	7848.00	29724.30
3	98.1	0.1000	0.0500	2.0000	7504.65	29783.16
4	98.1	0.1000	0.0500	2.0000	7507.59	29783.16
5	98.1	0.1000	0.0500	2.0000	7507.49	29783.16
True value	98.1	0.1000	0.0500	2.0000	7507.49	29783.16

Table 4
Parameters of floor 2–5 in numerical example (Mokha's mechanism).

Storey (j)	C_j (kN.s/m)		K_j (MN/m)	
	True	Identified	True	Identified
5	6918.89	6918.60	19973.16	19973.16
4	6918.89	6918.50	22916.16	22916.16
3	7016.99	7016.60	23897.16	23897.16
2	7115.09	7114.80	27821.16	27821.16

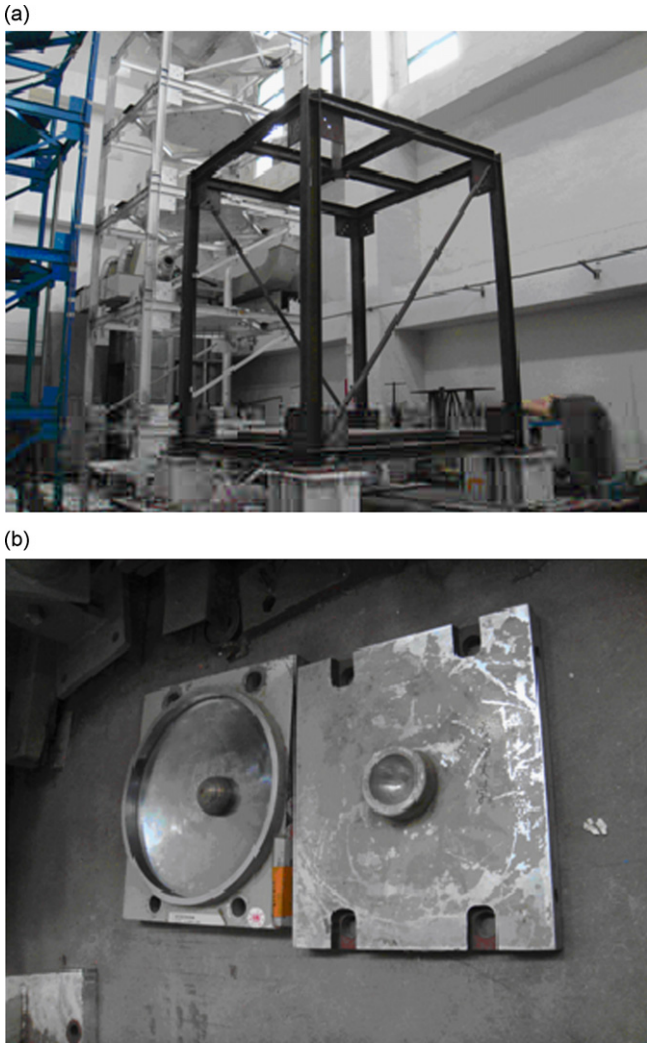

Fig. 5. (a) Test model of single-storey with FPS isolation system and (b) friction pendulum system used in the test.

The second cycle ($s=2$) is then proceeded with $C_1=8829.00$ kN.s/m determined in the first cycle, and the value of K_1 is increased by an increment of $\Delta K_1^{(2)}=\Delta K_1^{(1)}/10=98.1$ MN/m. The optimal estimate of K_1 is found to be 29724.30 MN/m. With K_1 fixed at 29724.30 MN/m and C_1 increased by an increment of $\Delta C_1^{(2)}=\Delta C_1^{(1)}/10=98.1$ kN.s/m, the optimal estimate of C_1 is found to be 7848.00 kN.s/m also at $a=98.1$. Meanwhile, the other parameters of the FPSs are found to be $\mu_{max}=0.0998$, $\mu_{min}=0.0499$, and $R=2.0025$ m.

The identification results converge to the true values again in five cycles as summarized in Table 3. The parameters for floor 2–5 of the superstructure are then calculated with an excellent accuracy as summarized in Table 4.

6. Experimental verification

As a further step in verifying the feasibility of the proposed scheme for identification of FPS-isolated structures utilizing seismic data, a shaking table test has been conducted using a single-story steel frame (Fig. 5(a)) with its base isolated by four FPS bearings (Fig. 5(b)). The structure is 2.6 m in height and approximately 17658 kN in weight. The 1940 El Centro earthquake is considered as the input excitation. Acceleration responses of the base and roof have been recorded during the test. The corresponding velocity and displacement responses are obtained through numerical integrations of the accelerations with baseline corrections. Both the Coulomb's and Mokha's mechanism have been considered in the identification of the friction mechanism for the FPS.

6.1. Coulomb's mechanism

The first cycle ($s=1$) of the identification starts again with $C_1=0$. The value of K_1 is increased by an increment of $\Delta K_1^{(1)}=98.1$ MN/m from 0 to 3924 MN/m. The relationship between the overall measure-of-fit e and K_1 is shown in Fig. 6(a). The optimal estimate of K_1 is found to be 882.90 MN/m. With K_1 fixed at this value and C_1 increased by an

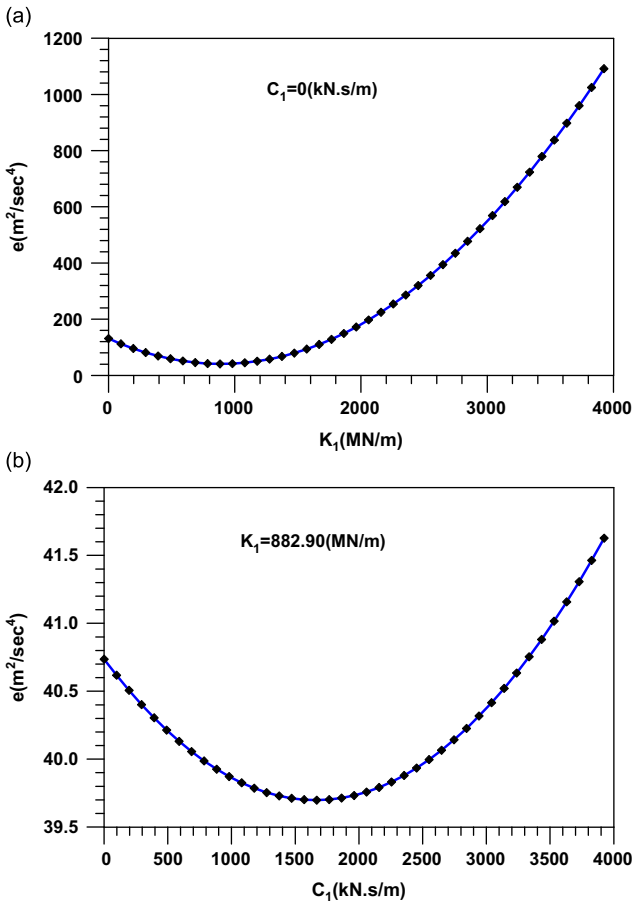

Fig. 6. (a) Measure-of-fit w.r.t. K_1 in the 1st cycle (Test; Coulomb's mechanism) and (b) measure-of-fit w.r.t. C_1 in the 1st cycle (Test; Coulomb's mechanism).

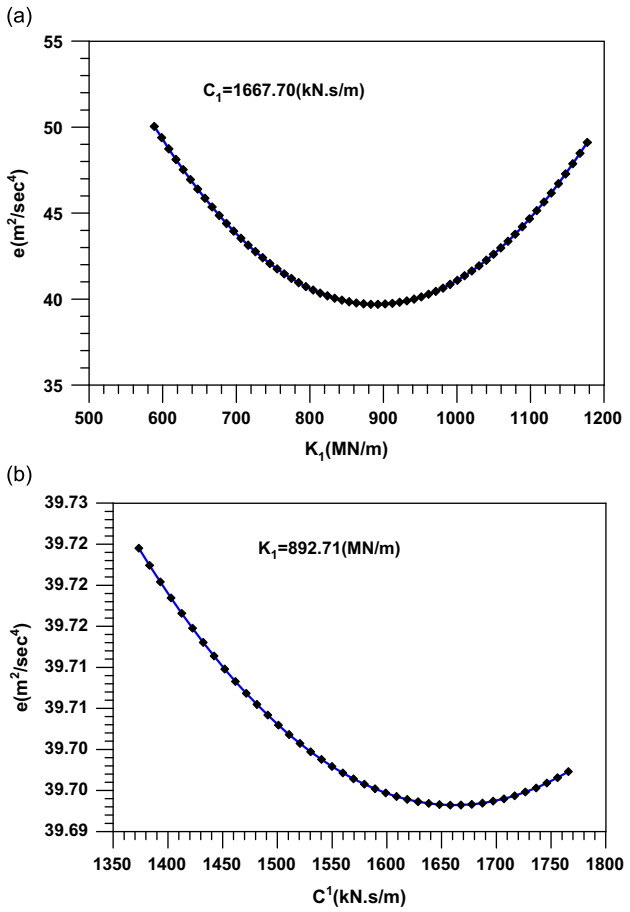

Fig. 7. (a) Measure-of-fit w.r.t. K_1 in the 2nd cycle (Test; Coulomb's mechanism) and (b) measure-of-fit w.r.t. C_1 in the 2nd Cycle (Test; Coulomb's mechanism).

Table 5
Parameters of FPS and floor 1 in the test (Coulomb's mechanism).

Iterative cycle (s)	FPS		Floor 1	
	μ	R (m)	C_1 (kN.s/m)	K_1 (MN/m)
1	0.0965	1.3015	1667.70	882.90
2	0.0966	1.3030	1657.89	892.71
3	0.0965	1.3025	1661.81	889.77

increment of $\Delta C_1^{(1)} = 98.1$ kN.s/m from 0 to 3924 kN.s/m. The relationship between the overall measure-of-fit e and C_1 is plotted in Fig. 6(b). The optimal estimate of C_1 is found to be 1667.70 kN.s/m. Meanwhile, the parameters for the FPS are estimated to be $\mu = 0.0965$ and $R = 1.3015$ m.

The second cycle ($s = 2$) is then proceeded with $C_1 = 1667.70$ kN.s/m determined in the first cycle. With K_1 increased by an increment of $\Delta K_1^{(2)} = \Delta K_1^{(1)}/10 = 9.81$ MN/m from 588.6 to 1177.2 MN/m, the relationship between the overall measure-of-fit e and K_1 is illustrated in Fig. 7(a). The optimal estimate of K_1 is found to be 892.71 MN/m. With K_1 fixed at 892.71 MN/m and C_1 increased by an increment of $\Delta C_1^{(2)} = \Delta C_1^{(1)}/10 = 9.81$ kN.s/m from 1373.4 to 1765.8 kN.s/m. The relationship between the overall measure-of-fit e and C_1 is plotted in Fig. 7(b). The optimal estimate of C_1 is found to be 1657.89 kN.s/m. Meanwhile, the parameters for FPSs are estimated to be $\mu = 0.0966$ and $R = 1.3030$ m.

The identification process converges in three cycles as summarized in Table 5. Fig. 8(a) and (b) shows the comparisons of the recorded with the predicted base acceleration and displacement using the identified system parameters. The responses are well correlated with each other in trends but differ in amplitudes. The predicted base displacement is overestimated with a larger residual off-set after 15 s when the excitation starts to quiet down. The largest discrepancy

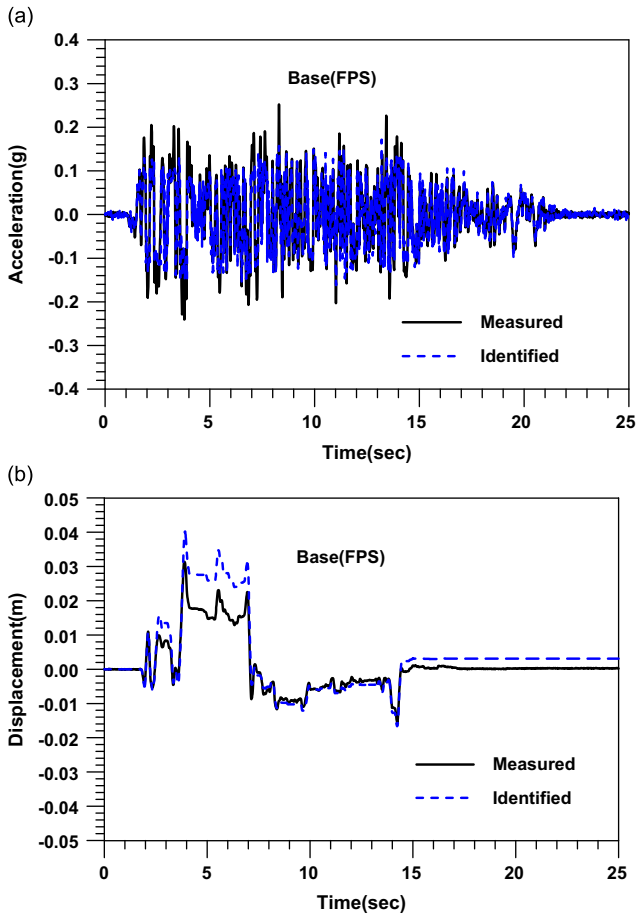

Fig. 8. (a) Comparison between identified and measured base acceleration (Test; Coulomb's mechanism) and (b) comparison between identified and measured base displacements (Test; Coulomb's mechanism).

Table 6
Parameters of FPS and floor 1 in the test (Mokha's mechanism).

Iterative cycle (s)	FPS				Floor 1	
	a	μ_{max}	μ_{min}	R (m)	C_1 (kN.s/m)	K_1 (MN/m)
1	382.59	0.1167	0.0552	1.4906	981.00	882.90
2	382.59	0.1167	0.0549	1.4885	882.90	873.09
3	382.59	0.1167	0.0550	1.4894	853.47	875.05
4	382.59	0.1167	0.0550	1.4892	856.41	874.56

occurs during the course of 3.5–7 s when the ground motion strikes most violently. This indicates that the Coulomb's mechanism of a constant friction is insufficient and the overall friction force is underestimated.

6.2. Mokha's mechanism

To begin with, $\Delta a=9.81$ and $a^0=0$ are considered in $a^l=a^{l-1}+\Delta a$ where l is set to be 50 in this case. The first cycle ($s=1$) starts with $C_1=0$. The value of K_1 is increased by an increment of $\Delta K_1^{(1)}=98.1$ MN/m. The optimal estimate of K_1 is found to be $K_1=882.90$ MN/m. Next, with K_1 fixed at this value and C_1 increased by an increment of $\Delta C_1^{(1)}=981$ kN.s/m, the optimal estimate of C_1 is found to be 981.0 kN.s/m at $a=382.59$. Meanwhile, the other parameters for the FPS are found to be $\mu_{max}=0.1167$, $\mu_{min}=0.0552$, and $R=1.4906$ m.

The second cycle ($s=2$) is then proceeded with $C_1=981.0$ kN.s/m determined in the first cycle. With K_1 increased by an increment of $\Delta K_1^{(2)}=\Delta K_1^{(1)}/10=9.81$ MN/m, the optimal estimate of K_1 is found to be 873.09 MN/m. Next, withK_1 fixed at this value and C_1 increased by an increment of $\Delta C_1^{(2)}=\Delta C_1^{(1)}/10=98.1$ kN.s/m, the optimal estimate of C_1 is found to be

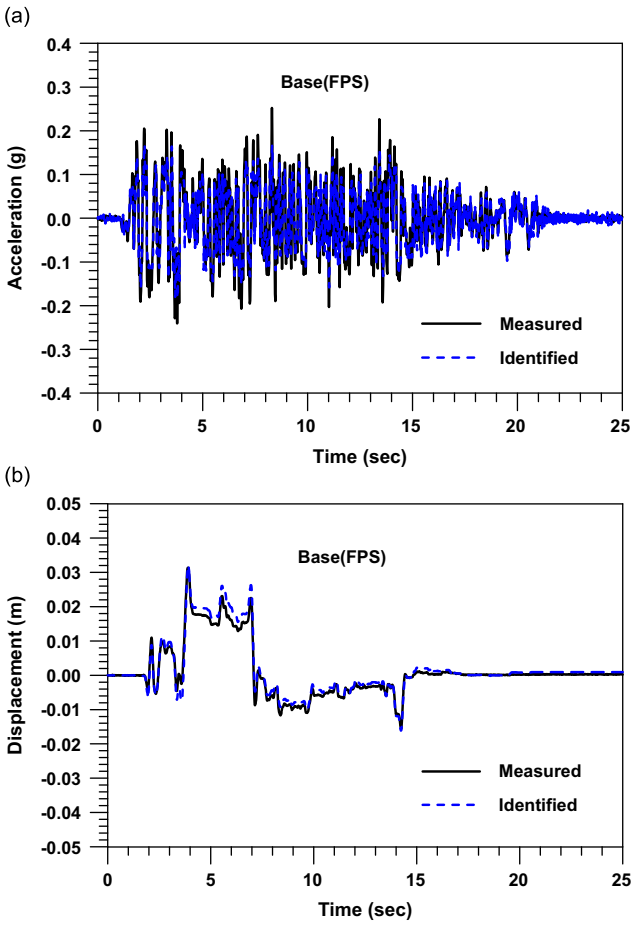

Fig. 9. (a) Comparison between identified and measured base acceleration (Test; Mokha's mechanism) and (b) comparison between identified and measured base displacements (Test; Mokha's mechanism).

882.9 kN.s/m at $a=382.59$. Meanwhile, the other parameters for the FPSs are found to be $\mu_{max}=0.1167$, $\mu_{min}=0.0549$, and $R=1.4885$ m.

The identification process converges in four cycles as summarized in Table 6. Fig. 9(a) and (b) shows the comparisons of base acceleration and displacement. With Mokha's mechanism considered for the friction, the responses are well correlated with each other in both trends and amplitudes with nearly no residual off-set. The result suggests that Mokha's friction mechanism describe the friction behavior better than Coulomb's mechanism does as it takes into account the variation of the friction coefficient due to sliding velocity and pressure.

7. Conclusion

A physical parameter identification scheme has been proposed for structures isolated with FPS using seismic response data. Both Coulomb's and Mokha's mechanism have been considered for the friction behavior of the FPS. Numerical and experimental studies have been conducted on shear-type structures to verify the proposed scheme. It has been verified that the system parameters of the superstructure and FPS can be effectively identified, regardless of Coulomb's or Mokha's mechanism considered. The predicted results based on the identified parameters from the test are in good agreement with the recorded data. They are, in particular, well correlated with each other in both trends and amplitudes when Mokha's mechanism is considered. This suggests that Mokha's mechanism is sufficient in describing the friction behavior of the isolation bearings, while Coulomb's mechanism might be overly simplified. The proposed scheme with Mokha's mechanism may facilitate in-situ performance assessment of structures isolated with sliding-type isolation systems.

Acknowledgments

This work is partially supported by the National Science Council of Republic of China under contracts NSC98-2625-M-344-001 and NSC 99–2625-M-009-006.

References

[1] J.M. Kelly, A seismic base isolation: review and bibliography, *Soil Dynamics and Earthquake Engineering* 5 (3) (1986) 202–217.
[2] I.G. Buckle, R.L. Mayes, Seismic isolation history, application and performance-a world review, *Earthquake Spectra* 6 (2) (1990) 161–201.
[3] R.S. Jangid, J.M. Kelly, Base isolation for near fault motions, *Earthquake Engineering and Structural Dynamics* 30 (5) (2001) 691–707.
[4] P. Pan, D. Zamfirescu, M. Nakayasu, H. Kashiwa, Base-isolation design practice in Japan: Introduction to the post-Kobe approach, *Journal of Earthquake Engineering* 9 (1) (2005) 147–171.
[5] K.L. Ryan, A.K. Chopra, Estimating seismic demands for isolation bearings with building overturning effects, *Journal of Structural Engineering, ASCE* 132 (7) (2006) 1118–1128.
[6] L.R. Keri, K.C. Anil, Estimating seismic demands for isolation bearings with building overturning effects, *Journal of Structural Engineering, ASCE* 123 (7) (2006) 1118–1128.
[7] V.A. Matsagar, R.S. Jangid, Base isolation for seismic retrofitting of structures, *Practice Periodical on Structural Design and Construction, ASCE* 13 (4) (2008) 175–185.
[8] M.K. Shrimali, R.S. Jangid, Seismic response of liquid storage tanks isolated by sliding bearings, *Engineering Structures* 24 (7) (2002) 907–919.
[9] M.K. Shrimali, R.S. Jangid, Seismic analysis of base isolated liquid storage tank, *Journal of Sound and Vibrations* 275 (2004) 59–75.
[10] M.K. Shrimali, S.D. Bharti, S.M. Dumne, Seismic response analysis of adjacent buildings connected with MR dampers, *Engineering Structures* 32 (8) (2010) 1223–1235.
[11] V. Zayas, S.S. Low, S.A. Main, The FPS Earthquake Resisting System, Experimental Report, Report No. UCB/EERC-87/01, Earthquake Engineering Research Center, University of California, Berkeley, California, 1987.
[12] V. Zayas, S. Mahin, A simple pendulum technique for achieving seismic isolation, *Earthquake Spectra* 6 (1990) 317–333.
[13] A. Mokha, M.C. Constantiou, A.M. Reinhorn, Experimental study of friction pendulum isolation system, *Journal of Structural Engineering, ASCE* 117 (4) (1991) 1201–1217.
[14] A. Mokha, N. Amin, M.C. Constantiou, V. Zayas, Seismic isolation retrofit of large historic building, *Journal of Structural Engineering, ASCE* 122 (3) (1996) 298–308.
[15] P. Tsopelas, M.C. Constantinou, Y.S. Kim, S. Okamoto, Experimental study of FPS system in bridge seismic isolation, *Earthquake Engineering and Structural Dynamics* 25 (1) (1996) 65–78.
[16] J.L. Almazan, J.C. De la Llera, J.A. Inaudi, Modeling aspects of structures isolated with the frictional pendulum system, *Earthquake Engineering and Structural Dynamics* 27 (1998) 845–867.
[17] J.L. Almazan, J.C. De la Llera, Analytical model of structures with frictional pendulum isolators, *Earthquake Engineering and Structural Dynamics* 31 (2002) 305–332.
[18] J.L. Almazan, J.C. De la Llera, Physical model for dynamic analysis of structures with FPS isolations, *Earthquake Engineering and Structural Dynamics* 32 (2003) 1157–1184.
[19] G. Mosqueda, A.S. Whittaker, G.L. Fenves, Characterization and modeling of friction pendulum bearings subjected to multiple components of excitation, *Journal of Structural Engineering, ASCE* 130 (3) (2004) 433–442.
[20] A. Kartoum, M.C. Constantinou, A.M. Reinhorn, Sliding isolation system for bridges: Analytical study, *Earthquake Spectra* 8 (3) (1992) 345–372.
[21] Y.P. Wang, L.L. Chung, W.H. Liao, Seismic response analysis of bridges isolated with friction pendulum bearings, *Earthquake Engineering and Structural Dynamics* 27 (10) (1998) 1069–1093.
[22] Y.P. Wang, M.C. Teng, K.W. Chuang, Seismic isolation of rigid cylindrical tanks using friction pendulum bearings, *Earthquake Engineering and Structural Dynamics* 30 (2001) 1083–1099.
[23] S. Ates, A. Bayraktar, A.A. Dumanoglu, The effect of spatially varying earthquake ground motions on the stochastic response of bridges isolated with friction pendulum system, *Soil Dynamics and Earthquake Engineering* 26 (1) (2006) 31–44.
[24] M.C. Kunde, R.S. Jangid, Effects of pier and deck flexibility on the seismic response of isolated bridge, *Journal of Bridge Engineering* 11 (1) (2006) 109–121.
[25] R.S. Jangid, Stochastic response of bridges seismically isolated by friction pendulum system, *Journal of Bridge Engineering* 13 (4) (2008) 319–330.
[26] C.C. Marin-Artieda, A.S. Whittaker, M.C. Constantinou, Experimental study of the XY-friction pendulum bearing for bridge applications, *Journal of Bridge Engineering, ASCE* 14 (3) (2009) 193–202.
[27] Y.C. Kim, X. Suduo, Z. Peng, Z. Wei, L. Chenghao, Seismic isolation analysis of FPS bearings in spatial lattice shell structures, *Earthquake Engineering and Engineering Vibration* 9 (2010) 93–102.
[28] S. Nagarajaiah, S. Xiaohong, Response of base-isolated USC hospital building in Northridge earthquake, *Journal of Structural Engineering, ASCE* 126 (10) (2000) 1177–1186.
[29] S. Nagarajaiah, S. Xiaohong, Base-isolated FCC building: impact response in Northridge earthquake, *Journal of Structural Engineering, ASCE* 127 (9) (2001) 1063–1075.
[30] T. Furukawa, M. Ito, K. Izawa, M.N. Noori, System identification of base-isolated building using seismic response data, *Journal of Engineering Mechanics, ASCE* 131 (3) (2005) 268–275.
[31] N.D. Oliveto, G. Scalia, G. Oliveto, Dynamic identification of structural systems with viscous and friction damping, *Journal of Sound Vibration* 318 (2008) 911–926.
[32] N.D. Oliveto, G. Scalia, G. Oliveto, Time domain identification of hybrid base isolation system using free vibration tests, *Earthquake Engineering and Structural Dynamics* 39 (2010) 1015–1038.
[33] A. Alleyne, J. Hedrick, Nonlinear adaptive control of active suspensions, *IEEE Transactions on Control Systems Technology* 3 (1) (1995) 94–101.
[34] W. Sun, H. Gao, O. Kaynak, Adaptive backstepping control for active suspension systems with hard constraints, *IEEE Transactions on Mechatronics,* Digital Object Identifier: 10.1109/TMECH.2012.2204765.
[35] A.S. Mokha, M.C. Constantinou, A.M. Reinhorn, Teflon bearing in base isolation. I: Testing, *Journal of Structural Engineering, ASCE* 116 (2) (1990) 438–454.
[36] A.S. Mokha, M.C. Constantinou, A.M. Reinhorn, Teflon bearing in base isolation. I: Modeling, *Journal of Structural Engineering, ASCE* 116 (2) (1990) 455–474.
[37] N.M.M. Maia, J.M.M. Silva (Eds.), *Theoretical and experimental modal analysis*, Research Studies Press Ltd., Taunton, U K, 2003.
[38] M.T.A. Chaudhary, M. Abe, Y. Fujino, J. Yoshida, System identification of two base-isolated bridges using seismic records, *Journal of Structural Engineering, ASCE* 126 (10) (2000) 1187–1195.